



## ORIGINAL RESEARCH COMMUNICATION

# TRPC6 Channel Regulates Airway Remodeling in Chronic Obstructive Pulmonary Disease Causing Right Heart Failure

Kun Liu,<sup>1,\*</sup> Qi-Ming Tan,<sup>2,\*</sup> Jie Zhang,<sup>1</sup> Gong-Hao Li,<sup>1</sup> and Yun-Feng Zhao<sup>1</sup>

### Abstract

The role of the canonical transient receptor potential 6 (TRPC6) channel in chronic obstructive pulmonary disease (COPD) remains poorly understood at the mechanistic level.

**Objects:** This study aims to investigate the involvement of TRPC6 in COPD and its signaling mechanisms in human airway smooth muscle cells (HASMCs).

**Methods and Results:** The study found that mRNA and protein expression of TRPC6 increased in cultured HASMCs that were incubated with nicotine, as measured by reverse transcription quantitative polymerase chain reaction and Western blot analysis. Nicotine treatment significantly enhanced TRPC6 transcriptional activity in HASMCs through nuclear factor (NF)- $\kappa$ B, as demonstrated by co-immunoprecipitation and electrophoretic mobility shift assays. Furthermore, miR-135a/b-5p was shown to downregulate TRPC6 expression in HASMCs at the mRNA and protein levels, as confirmed by luciferase reporter assays. Immunohistochemistry assays in a mouse model of cigarette-induced airway remodeling revealed a significant increase in smooth muscle (SM) cell proliferation and SM layer mass.

**Conclusion:** These findings suggest that nicotine exposure increases HASMC proliferation and migration through NF- $\kappa$ B signaling, and that cigarette smoke inhalation causes airway SM layer remodeling *via* altered TRPC6-induced  $\text{Ca}^{2+}$  influx, which is abolished by miR-135a/b-5p both *in vitro* and *in vivo*. *Antioxid. Redox Signal.* 00, 000–000.

**Keywords:** TRPC6, miR-135a/b-5p, NF- $\kappa$ B, airway remodeling, COPD, right heart failure

### Introduction

Chronic obstructive pulmonary disease (COPD) is a progressive and diverse lung condition characterized by persistent airway remodeling, airflow limitation, and chronic pulmonary inflammation. It lacks effective treatments and is a leading cause of death in the United States and worldwide (Mannino and Buist, 2007). The primary risk factor for COPD is exposure to cigarette smoke, which contains harmful inflammatory and oxidant agents (Tannus-Silva and Rabahi, 2017). In COPD, calcium ion ( $\text{Ca}^{2+}$ ) signaling is considered a crucial feature for the proliferation and migration of airway smooth muscle cells (ASMCs) (Ten Broeke et al., 2004). The TRPC channel is a nonselective cation channel that facilitates the entry of  $\text{Ca}^{2+}$  and sodium ions ( $\text{Na}^{+}$ ) and is involved in

multiple intracellular signaling pathways. It regulates various cellular functions dependent on  $\text{Ca}^{2+}$ , from cell growth to myocyte contraction. Among the canonical transient receptor channel (TRPC) family, there are at least seven members (TRPC1–7) that mediate various signal transduction pathways (Svobodova and Groschner, 2016; Liao et al., 2009; Xu et al., 2008). A particularly significant member is the TRPC6 channel, which is widely expressed in various organs, including the kidney, placenta, lung, heart, brain, skin, and vasculature (Boulay et al., 1997; Garcia and Schilling, 1997; Riccio et al., 2002; Müller et al., 2008). Evidence indicates that TRPC6 plays a crucial role in normal lung function and disease states of the pulmonary vasculature. In pulmonary artery smooth muscle cells,  $\text{Na}^{+}$  influx through TRPC6 channels leads to membrane depolarization and the activation of voltage-gated L-type  $\text{Ca}^{2+}$  channels. This, in

<sup>1</sup>Department of Cardiology, The First People's Hospital of Lianyungang, The Affiliated Lianyungang Hospital of Xuzhou Medical University, Lianyungang, China.

<sup>2</sup>Department of Cardiac Surgery, The First People's Hospital of Lianyungang, The Affiliated Lianyungang Hospital of Xuzhou Medical University, Lianyungang, China.

\*These authors contributed equally to this work as first authors.

## Innovation

We found that cigarette smoke inhalation causes airway SM layer remodeling *via* altered TRPC6-induced  $\text{Ca}^{2+}$  influx. Nicotine triggered the signaling cascades, leading to the translocation of p65 and p50 through the  $\alpha 7$  nAChR and reactive oxygen and nitrogen species-dependent pathway in HASMCs. This led to the sustained activation of transcriptional signaling, increasing TRPC6 expression, and a decrease in miR-135a/b-5p. The direct influx of  $\text{Ca}^{2+}$  was activated, followed by the induction of downstream gene activation of NFAT signaling, leading to HASMC proliferation and migration. These findings provide a new perspective on the mechanism research of airway remodeling and offer new targets for the treatment of COPD.

turn, mediates the bulk of the  $\text{Ca}^{2+}$  influx and smooth muscle cell contraction (Weissmann et al., 2006) (Gudermann et al., 2004). Therefore, TRPC6 channels may serve as a potential therapeutic target for managing pulmonary hemodynamics and gas exchange in both physiological and pathological conditions.

The miR-135 family is highly conserved among mammals and consists of two members, miR-135a and miR-135b, that have been shown to directly regulate the expression of several genes, including TRPC1 (He et al., 2014), HOXA10 (Tang et al., 2014), and c-myc (Yamada et al., 2013). Despite these findings, the exact functions of the two miR-135 family members, especially their role in smoking-related lung diseases, remain unclear. Through microRNA research assays, this study identified that miR-135a/b-5p post-transcriptionally regulates TRPC6 expression and plays a crucial role in the proliferation of human airway smooth muscle cells (HASMCs) following exposure to nicotine.

## Results

### *The proliferation and migration of ASMCs from patients with COPD are mediated by TRPC6 channels*

To investigate the effect of TRPC6 on the proliferation of HASMCs, normal and COPD HASMCs were isolated and cultured. The cells were plated at a low confluence and monitored for cell proliferation over several days by measuring absorbance at 490 nm after adding MTS solution. Results showed that COPD HASMCs were more proliferative than normal HASMCs (Fig. 1A). Moreover, TRPC6 overexpression facilitated the proliferation of normal HASMCs (Fig. 1B). Conversely, both TRPC6 knockdown and inhibition using SAR 7334 suppressed COPD HASMCs growth (Fig. 1C). The expression level of TRPC6 protein was found to be significantly higher in COPD HASMCs than in normal HASMCs (Fig. 1D). In addition, knockdown of the TRPC6 channel protein showed a notable decrease in transwell migration in COPD HASMCs (Fig. 1G). Western blot analysis confirmed the efficient upregulation (Fig. 1E) and downregulation (Fig. 1F) of TRPC6 protein.

### *Hsa-miR-135a/b-5p plays an essential role in regulating the expression and activity of TRPC6 in COPD human ASMCs*

We aimed to identify specific microRNAs that could modulate TRPC6 expression, focusing on the regulatory mechanisms

and biological significance of TRPC6 in HASMCs. miR-135a/b-5p has been predicted to target on the 3'-UTR of TRPC6 mRNA. Among the top six microRNAs that were downregulated in lungs from patients with COPD compared with smokers without COPD (Ezzie et al., 2012) and six microRNAs that were predicted to bind to TRPC6-3'-UTR based on the "microRNA.org" algorithm (<http://www.microrna.org/>) (Supplementary Table S1), indeed, miR-135a/b-5p were shown to decrease TRPC6 expression in 293T cells compared with other microRNAs by Western blot analysis (Fig. 2A). Transfection with miR-135a/b-5p mimics reduced TRPC6 mRNA and protein expression, regardless of normal or COPD HASMCs (Fig. 2B and 2E). Nicotine significantly increased the TRPC6 mRNA level in TRPC family members in normal HASMCs (Fig. 2F). To verify the effect of nicotine and miR-135a/b-5p on TRPC6 expression, HASMCs were treated with nicotine and transfected with miR-135a/b-5p mimics. In normal HASMCs, nicotine increased TRPC6 channel expression dramatically, and miR-135a/b-5p overexpression reduced TRPC6 protein expression faintly (Fig. 2C). In COPD HASMCs, nicotine increased TRPC6 channel expression faintly, while miR-135a/b-5p overexpression reduced TRPC6 protein dramatically (Fig. 2D). The probable explanation is TRPC6 expression was high in COPD patients than normal. To identify the regulatory sequence in 3'-UTR of TRPC6, full-length (FL) and two additional reporters with a truncated sequence in 3'-UTR of TRPC6 were established. A computational search predicted the site of miR-135a/b-5p binding to the TRPC6-3'-UTR (Fig. 2G). HEK-293T cells were co-transfected with miR-135a/b-5p mimics and pmiR-TRPC6-3'-UTR-FL or TRPC6-3'-UTR truncates, respectively. Luciferase reporter activity of TRPC6-3'-UTR-FL and TRPC6-3'-UTR-1–49 were decreased, and the TRPC6-3'-UTR-1–43 did not (Fig. 2H), suggesting the sequence from 43–49 of 3'-UTR of TRPC6 was essential to bind between miR-135a/b-5p and TRPC6 mRNA. In addition, decreased levels of the miR-135a/b-5p by nicotine (Supplementary Fig. S1) can further increase TRPC6 expression.  $\text{Ca}^{2+}$  release in the cytosol by nicotine treatment was attenuated by miR-135a/b-5p (Fig. 2I). These lines of evidence collectively demonstrated that miR-135a/b-5p recognized and regulated TRPC6 mRNA through binding to its 3'-UTR.

### *Nicotine is responsible for increasing the expression of TRPC6 through nuclear factor- $\kappa$ B*

In order to gain a better understanding of how HASMCs respond to nicotine stimulation at the molecular level, we conducted a genome-wide unbiased approach to analyze gene expression *via* RNA sequencing. Our analysis identified a profound impact on gene expression networks, with notable enrichments in gene sets corresponding to "BIOCARTA\_NFKB\_PATHWAY" and "BIOCARTA\_NFAT\_PATHWAY" (Fig. 3A). We observed that an  $\alpha 7$  nAChR inhibitor, MG 624, abolished the increase in nuclear factor (NF)- $\kappa$ B activity caused by nicotine (Fig. 3B). Furthermore, we observed a significant increase in NF- $\kappa$ B translocation and reduced levels of cytoplasmic NF- $\kappa$ B in response to nicotine treatment (Fig. 3C), supporting the promotional effects of nicotine on NF- $\kappa$ B translocation. Nicotine did not significantly change the TRPC6 protein level in HASMCs infected with lentivirus of p65\_sh and p50\_sh (NF- $\kappa$ B\_sh) (Fig. 3D). Similarly, treating HASMCs with the NF- $\kappa$ B inhibitor, BAY 11–7082, also yielded comparable results (Fig. 3E). We also found that nicotine increased TRPC6 mRNA level

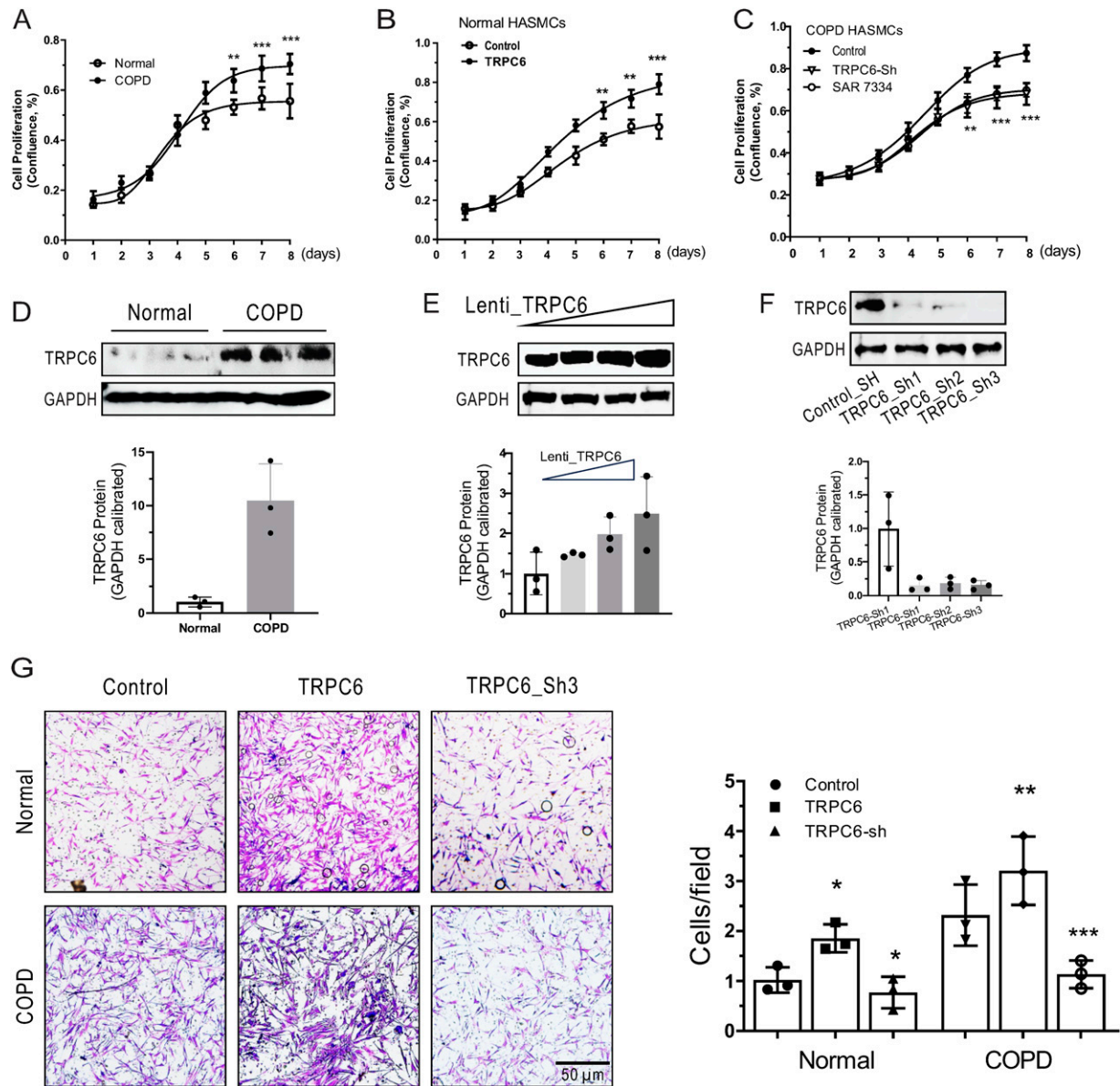


**FIG. 1. The effect of TRPC6 on the growth and mobility of normal and COPD ASMCs.** (A) The proliferation rate of COPD HASMCs was faster than that of normal HASMCs. HASMCs were obtained from healthy donors and patients with COPD and cultured for 1–8 days. The MTS assay was performed, and the experiment was repeated three times independently. (B) The lentiviral infection of TRPC6 promoted normal HASMC proliferation. The cells were infected with lentivirus containing TRPC6 and cultured for 1–8 days. Proliferation was analyzed through the MTS assay, and the experiment was repeated three times independently. (C) The knockdown and inhibition of TRPC6 resulted in a decrease in HASMC proliferation. COPD HASMCs were infected with lentivirus containing TRPC6\_Sh, or treated with SAR 7334 (1  $\mu$ M) for 1–8 days. The MTS assay was performed to analyze proliferation, and the experiment was repeated three times independently. (D) TRPC6 protein expression was higher in cultured COPD HASMCs than in normal HASMCs. HASMCs were isolated and cultured from the bronchia of control subjects and patients with COPD. (E) The overexpression and knockdown (F) of TRPC6 were achieved in HASMCs. The cells were infected with increasing lentiviral particles of Human\_TRPC6 or Human\_TRPC6\_Sh for 5 days. TRPC6 expression was analyzed through Western blotting. (G) COPD stimulated HASMC migration through TRPC6. Normal and COPD HASMCs were infected separately with lentivirus of TRPC6\_SH and TRPC6. Cell migration was analyzed through crystal violet dye staining of HASMCs that migrated into the transwell. The right panel features quantification, with data indicating the number of cells migrated in three experiments. Significance was determined as follows: \*,  $p < 0.05$ ; \*\*,  $p < 0.01$ ; \*\*\*,  $p < 0.001$ . COPD, chronic obstructive pulmonary disease; HASMCs, human airway smooth muscle cells; TRPC6, transient receptor potential channel 6.

in HASMCs while silencing NF- $\kappa$ B by knockdown or pharmacological inhibition abolished the nicotine-induced TRPC6 mRNA increase (Fig. 3F). To explore the possibility of the NF- $\kappa$ B binding site for TRPC6 expression, luciferase activity assays employing a luciferase reporter construct driven by the TRPC6

promoter sequence were performed in normal HASMCs. As shown in Figure 3G, both nicotine and NF- $\kappa$ B manipulation positively correlated with cellular TRPC6 transcriptional activity. Our data confirm that nicotine promotes TRPC6 mRNA and protein expression in an NF- $\kappa$ B-dependent mechanism. To



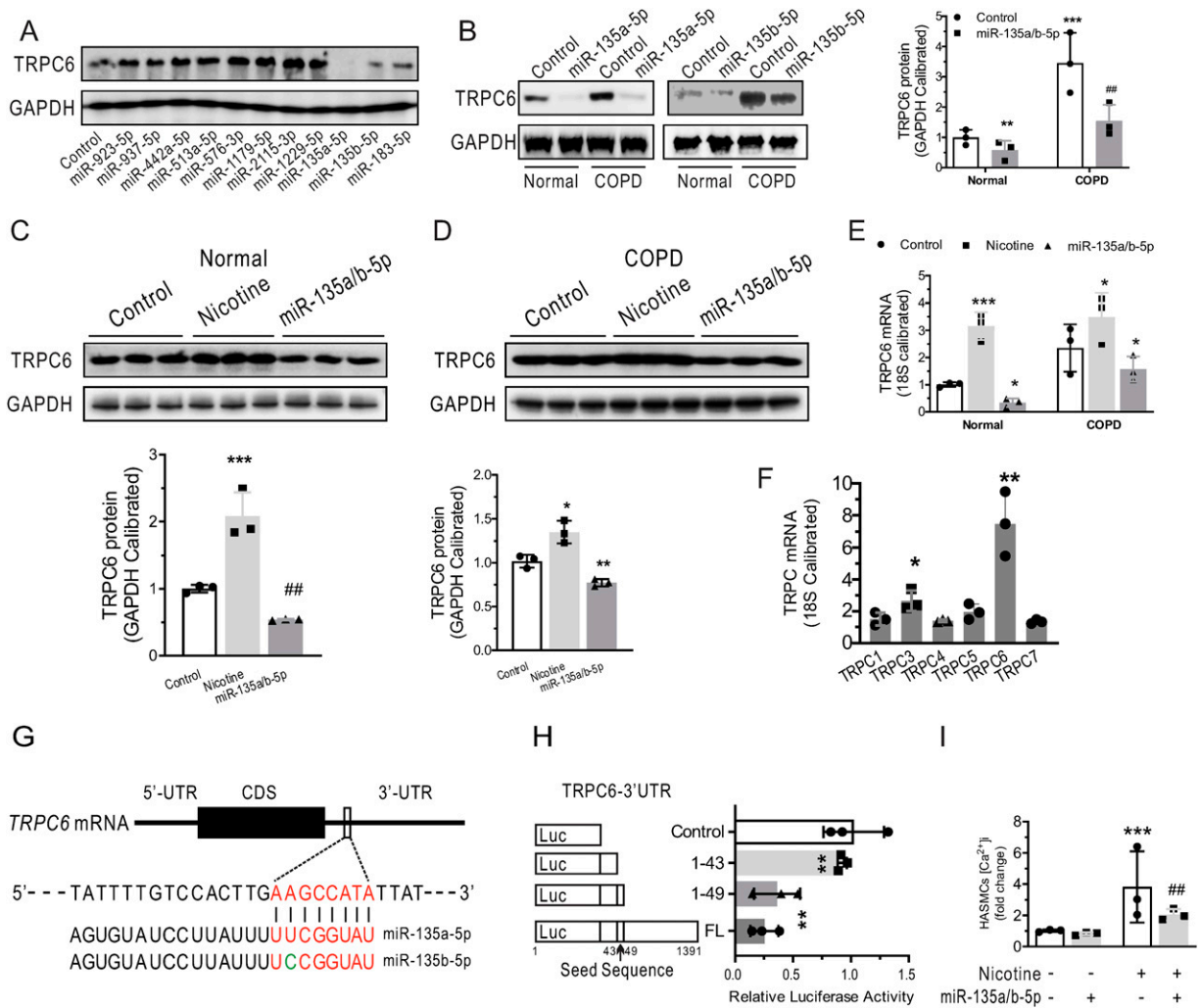


**FIG. 2. Hsa-miR-135a/b-5p inhibits the migration of ASMCs by degrading TRPC6 expression.** (A) Hsa-miR-135a/b-5p downregulated TRPC6 protein level in 293T cells. 293T cells were transfected with 12 microRNA mimics predicted to bind TRPC6 mRNA 3'-UTR. Western blotting was performed to analyze the TRPC6 expression, with GAPDH as the internal control. (B) MiR-135a/b-5p mimics reduced the protein expression and mRNA (E) levels of TRPC6 in normal, and COPD HASMCs. (C) Nicotine treatment (1  $\mu$ M) increases the protein levels of TRPC6 in normal and COPD (D) HASMCs. The mixture of hsa-miR-135a-5p and hsa-miR-135b-5p mimics (the ratio at 1:1) were transfected into the normal and COPD HASMCs from different donors for 24 h. Western blotting was performed to analyze the TRPC6 expression, with GAPDH as the internal control. (F) The mRNA expression of TRPC3 and TRPC6 was significantly higher in normal HASMCs treated with nicotine. Real-time qPCR and Western blotting were used to determine mRNA and protein expression, respectively, with 18S and GAPDH as the internal control. These experiments were repeated three times independently, with \* indicating  $p < 0.05$  and \*\*\* indicating  $p < 0.005$ . G. The targeting site for hsa-miR-135a/b-5p was identified in the TRPC6 3'-UTR. H. The TRPC6\_3'-UTR\_576-589 site is crucial for the binding between hsa-miR-135a/b-5p and TRPC6 mRNA. The pmir-target vector was cloned with two truncated and one full-length TRPC6\_3'-UTR, which were co-transfected with miR-135a/b-5p mimics into HEK-293T cells. Firefly luciferase expression was normalized to that of renilla luciferase. The experiments were repeated three times independently, and the results indicate that the TRPC6\_3'-UTR\_576-589 site is indispensable for the binding between hsa-miR-135a/b-5p and TRPC6 mRNA. I. Intracellular  $\text{Ca}^{2+}$  levels were detected in HASMCs treated with nicotine (1 nM) for 30 min after the transfection of miR-135a/b-5p mimics for 24 h. ASMCs, airway smooth muscle cells; qPCR, quantitative polymerase chain reaction.

verify the putative interaction between NF- $\kappa$ B and the NF- $\kappa$ B response element (NRE) of the TRPC6 promoter, we carried out electrophoretic mobility shift assays (EMSAs). As shown in Figure 3H, increasing exposure hours of nicotine significantly increased the intensity of the shifted band in the probe-shift assays. In supershift assays (Fig. 3I), incubation of p65 antibodies with HASMCs nuclear extract pre-incubated with biotin-

labeled wild-type probe resulted in the formation of a super-shifted band with a larger molecular weight than the shifted band, indicating the shape of an NRE-WT/p65/anti-p65 antibody complex. Furthermore, pre-incubation of the nuclear extract with a 200-fold excess of unlabeled WT probe completely diminished the shifted band, unlike a 200-fold excess of unlabeled mutant probes that failed to do so (Supplementary Fig. S3A). In

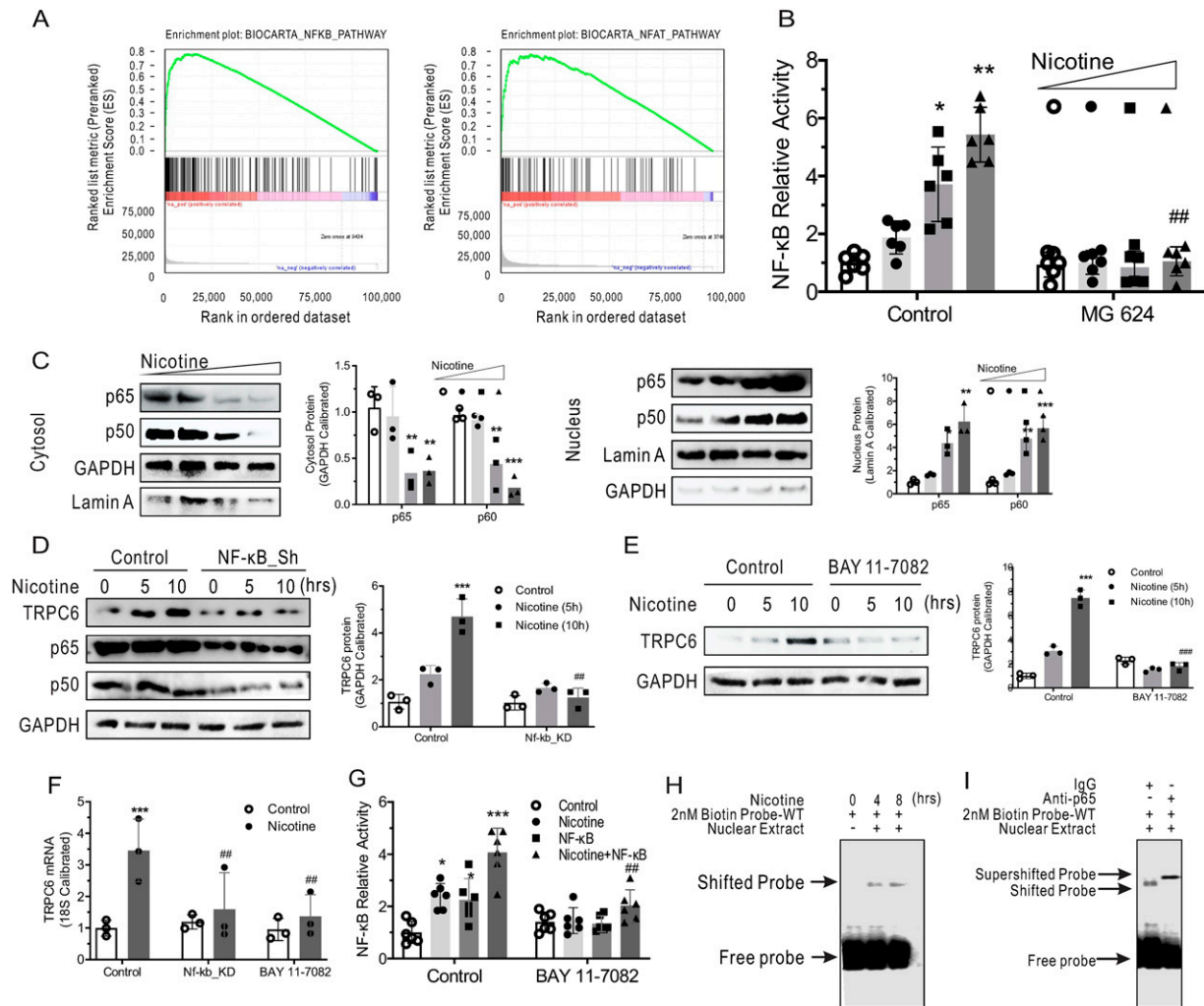


**FIG. 3. Nicotine regulates TRPC6 expression through NF- $\kappa$ B.** (A) Using the GSEA BIOCARTA biological process, the nicotine treatment group ( $n = 3$ ) showed significant enrichment in the “BIOCARTA\_NFKB\_PATHWAY” and “BIOCARTA\_NFAT\_PATHWAY” signatures. (B) The HASMCs transfected with NF- $\kappa$ B luciferase reporter plasmid were treated with a specific  $\alpha 7$  nAChR inhibitor, MG 624 (1  $\mu$ M), and firefly luciferase activity was measured and normalized to renilla luciferase. (C) Nicotine administration at various concentrations (0, 1, 10, and 100 nM) promoted the translocation of p50 and p65 into the nucleus. Cytoplasmic and nuclear fractions were separated by SDS-PAGE and immunoblotted with specific antibodies. GAPDH and Lamin A antibodies were used to control for cytoplasmic and nuclear proteins, respectively. Each experiment was repeated three times. (D) NF- $\kappa$ B knockdown attenuates nicotine-induced TRPC6 protein increase in HASMCs. Normal HASMCs were infected with lentivirus of p65\_Sh and p50\_Sh and stimulated with nicotine (100 nM) as indicated hours. (E) Inhibition of NF- $\kappa$ B abolishes nicotine-induced TRPC6 protein increase in HASMCs. Normal HASMCs were pre-treated with the NF- $\kappa$ B inhibitor BAY 11-7082 (1  $\mu$ M) and stimulated with nicotine (100 nM) as indicated hours. Protein expression was determined by immunoblotting. (F) TRPC6 mRNA level is upregulated by nicotine treatment in HASMCs, and this increase is dependent on NF- $\kappa$ B. HASMCs were infected with lentivirus of p65\_Sh and p50\_Sh or treated with BAY 11-7082 (1  $\mu$ M) and stimulated with nicotine (100 nM). Real-time qPCR analysis was performed with 18S as the internal control. (G) Nicotine promotes NF- $\kappa$ B binding to the TRPC6 promoter. TRPC6 promoter-reporter gene plasmids and NF- $\kappa$ B overexpression plasmids were transfected into HASMCs. After treatment with nicotine (100 nM) and the NF- $\kappa$ B inhibitor BAY 11-7082 (1  $\mu$ M), TRPC6 promoter reporter luciferase activity was measured. Firefly luciferase activity was normalized to renilla luciferase. (H) Electrophoretic mobility shift assays demonstrate an interaction between NF- $\kappa$ B and the NF- $\kappa$ B binding site of the TRPC6 promoter in HASMCs. HASMCs were stimulated with nicotine (100 nM) for 0, 4, and 8 h, and cells were harvested for gel-shift and supershift assay analysis (I), showing a significant binding of NF- $\kappa$ B to the TRPC6 promoter. \*\*\* $p < 0.001$ , compared with the control group; ## $p < 0.01$  compared with the nicotine group. NF- $\kappa$ B, nuclear factor- $\kappa$ B; GSEA, Gene Set Enrichment Analysis.

addition, incubation of the nuclear extract with a biotin-labeled mutant probe (NRE-MUT) did not result in any shifted band (Supplementary Fig. S3B). Moreover, pre-incubation of the nuclear extract with a biotin-labeled MUT probe did not prevent

the formation of the shifted band after subsequent incubation with a biotin-labeled WT probe. Together, these data demonstrate the interaction of NF- $\kappa$ B with NRE-WT in the TRPC6 promoter in HASMCs.

*Nicotine activates NF- $\kappa$ B transcriptional activity and TRPC6 activity through a reactive oxygen and nitrogen species-dependent manner*

We investigated the effects of NADPH oxidase using inhibitor apocynin (Stolk et al., 1994) as well as the potential role of mitochondrial complex (I inhibitor: rotenone; and III preubismiquinone site inhibitor: myxothiazol) on the nicotine stimulus in reactive oxygen species (ROS) levels in HASMCs. Using a specific cell-permeable red fluorescence dye (Fig. 4A and Supplementary Fig. S2B) and H2DCFDA green fluorescence dye (Supplementary Fig. S2A), we observed, pretreatment with apocynin, myxothiazol, or rotenone significantly blocked the nicotine-induced ROS levels increase in HASMCs (Fig. 4A and Supplementary Fig. S2A and S2B). Inhibition of ROS by using a hydroxyl radical (HO $\bullet$ ) scavenger, mannitol, or the superoxide dismutase, attenuated nicotine-induced Ca<sup>2+</sup> influx (Fig. 4B). Although the NO-sGC-cGMP pathway is a central signaling in cardiopulmonary regulation (Benza et al., 2024), the autonomous role of nicotine in the NO-mediated sGC/cGMP pathway in HASMCs remains unclear. The nicotine treatment in HASMCs augmented the NO<sub>2</sub><sup>-</sup> level, as determined by quantification of NO<sub>2</sub><sup>-</sup> production using the Griess reaction (Fig. 4C). Nitric oxide (NO) released from endothelial cells promotes smooth muscle relaxation through the cGMP pathway (Benza et al., 2024). Unlike in vascular smooth muscle cells, we found that NO level increases caused by nicotine did not change cGMP production in HASMCs (Supplementary Fig. S2C). However, inhibition of NO<sub>2</sub><sup>-</sup> by using a reactive nitrogen species (RNS) scavenger, carboxy-PTIO, and an iNOS inhibitor N(6)-(1-iminoethyl)-L-lysine, L-NIL, attenuated nicotine-induced Ca<sup>2+</sup> influx (Fig. 4D). Moreover, NO donors also partly replicate the effects of nicotine stimulation. Constant NO delivery of NO by ( $\pm$ )-S-nitroso-N-acetylpenicillamine (Wu et al., 2002) and slow release of NO by NOC-18 (Kano et al., 2000) provide a continuous flux of NO to HASMCs, then increase the level of calcium ions (Fig. 4E). We also observed that partial clearance of reactive oxygen and nitrogen species (RONS) by a hydroxyl radical (HO $\bullet$ ) scavenger, mannitol or RNS scavenger, carboxy-PTIO, abolished the increase in nicotine-caused NF- $\kappa$ B activity increase (Fig. 4F). In conclusion, our data support the idea that nicotine promotes NF- $\kappa$ B transcriptional activity and TRPC6 activity through an RONS-dependent manner in HASMCs.

TRPC6 channel activity was activated by NO, which may also be through cysteine S-nitrosylation on the N-terminal side of the pore region (Yoshida et al., 2006).

*Cigarette smoke activates nuclear factor of activated T-cell signaling in MASCs, causing ASM hyperresponsiveness and remodeling in a mouse model*

Furthermore, the inhalation of cigarette smoke has been found to enhance the methacholine-induced increase in airway resistance and contraction. However, the tail vein injection of lentivirus of SMC-specific TRPC6\_shRNAs effectively abolished this enhancement in mice with cigarette-evoked airway disease, as evident from Figure 5A and 5B. Moreover, cigarette smoke was observed to result in a significant increase in nuclear factor of activated T-cells (NFAT) and its target gene expression, but the silencing of TRPC6 specifically abrogated this gene expression increase caused by cigarettes, as shown in

Figure 5C (RT-qPCR primers see Supplementary Table S2). In addition, cigarette-inhaled mice demonstrated a significant increase in ASM mass and cell proliferation, as determined by  $\alpha$ -SMC actin and Ki67 immunohistochemistry staining. This well-characterized airway remodeling, which manifests in increased thickness of ASM layer and the number of Ki67-positive cells, was eliminated by tail vein injection of lentivirus of SMC-specific TRPC6\_shRNAs, as depicted in Figure 5D. Overall, these results establish that the lentivirus of SMC-specific TRPC6\_shRNAs can specifically knockdown the TRPC6 protein in ASMCs, thereby blocking cigarette-induced airway hyper-responsiveness and remodeling.

*miR-135a/b-5p has a mitigating effect on airway hyperresponsiveness and remodeling in a distinct murine model of asthma-COPD overlap syndrome*

Notably, certain patients with COPD display clinical and pathological overlap with those having asthma, suggesting underlying similarities between the two conditions (Christenson et al., 2015). The presence of methacholine can induce airway resistance and contraction. Tail vein injection of the lentivirus of miR-135a/b-5p effectively abolished ovalbumin and cigarette-evoked airway hyperresponsiveness in mice, consistent with TRPC6 knockdown (Fig. 6A and 6B). Moreover, ovalbumin-treated mice inhaling cigarettes exhibited a significant increase in ASM mass and HASMC proliferation, as determined by  $\alpha$ -SMC actin and Ki67 immunohistochemistry staining. However, this well-characterized airway remodeling was effectively eliminated by tail vein injection of lentivirus of miR-135a/b-5p, as shown in Figure 6C.

*The TRPC6 channel protein expression and airway thickness increase in ASM tissues from patients with COPD simultaneously*

To investigate the TRPC6 protein expression in normal and COPD bronchial smooth muscle tissues, a Western blot assay was performed to show that the protein was significantly upregulated in the COPD group by  $\sim$ two-fold compared with the normal group (Fig. 7A). In addition, immunohistochemical staining analysis with  $\alpha$ -SMC actin and TRPC6 antibodies revealed a higher percentage of TRPC6 protein-positive cells in COPD tissue samples (Fig. 7B). A correlation study also demonstrated that TRPC6 protein expression was proportional to the thickness of the bronchial smooth muscle layer (pink) (Supplementary Fig. S4).

*miR-135a/b-5p improves pulmonary vascular remodeling induced by cigarette smoke and ovalbumin*

The effects of miR-135a/b-5p on cigarette and ovalbumin-induced pulmonary vascular remodeling were assessed. Pathological evaluations of small pulmonary arteries (50–150  $\mu$ m) indicated increased wall thickness and luminal stenosis in the cigarette and ovalbumin group compared to controls. However, miR-135a/b-5p significantly alleviated these effects, as evidenced by a reduction in the thickening of the pulmonary artery wall (Fig. 8A). These findings suggest that miR-135a/b-5p significantly improved the pulmonary vascular remodeling induced by cigarette and ovalbumin. Further evaluations were performed using ultrasound to examine the right ventricular dimensions and systolic function in mice. The results showed a significant increase in the RVEDD of the Cig+Ova group and



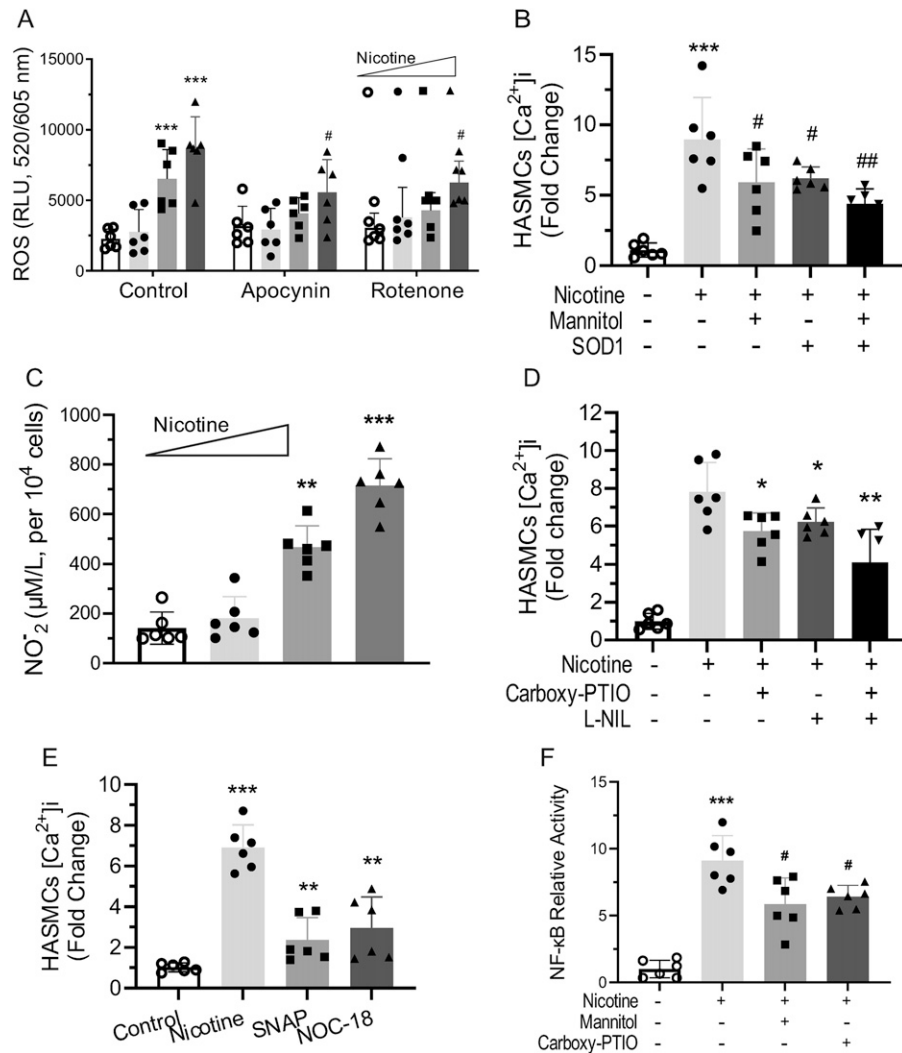


**FIG. 4. Nicotine activates NF- $\kappa$ B signaling and TRPC6 activity through RONS.** (A) HASMCs were treated with increasing concentrations of nicotine (0, 1, 10, and 100 nM) alone, nicotine combination of NADPH oxidase, apocynin (1  $\mu$ M), or mitochondrial electron transport chain complex I inhibitor rotenone (1  $\mu$ M) for 24 h. Intracellular ROS was quantified using a specific cell-permeable red fluorescence dye, and the assay was performed by microplate fluorometry (Ex/Em = 520/605 nm). (B) Intracellular Ca<sup>2+</sup> levels were detected in HASMCs treated with nicotine (100 nM) alone, nicotine combination of hydroxyl radical (HO $\bullet$ ) scavenger, mannitol (1  $\mu$ M), or SOD1 transfection for 24 h. (C) The NO<sub>2</sub><sup>-</sup> levels upon nicotine increase (0, 1, 10, and 100 nM) were determined in HASMCs culture supernatants by the Griess reaction. (D) Intracellular Ca<sup>2+</sup> levels were detected in HASMCs treated with nicotine (100 nM) alone, nicotine combination of a NO scavenger, carboxy-PTIO (1  $\mu$ M), or a specific iNOS inhibitor, N(6)-(1-iminoethyl)-L-lysine (L-NIL, 1  $\mu$ M) for 24 h. (E) Intracellular Ca<sup>2+</sup> levels were detected in HASMCs treated with nicotine (100 nM), NO donor, ( $\pm$ )-S-nitroso-N-acetylpenicillamine (SNAP, 1  $\mu$ M), or NOC18 (1  $\mu$ M) for 24 h. (F) HASMCs were treated with nicotine (100 nM), nicotine combination of ROS scavenger, mannitol (1  $\mu$ M) or NO scavenger, carboxy-PTIO (1  $\mu$ M) for 24 h, NF- $\kappa$ B luciferase activity was measured and normalized to renilla luciferase in HASMCs. Data were replicated in six independent experiments. \* $p$  < 0.05, \*\* $p$  < 0.01, \*\*\* $p$  < 0.001, compared with the control group; # $p$  < 0.05, ## $p$  < 0.01 compared with the nicotine group. ROS, reactive oxygen species; RONS, reactive oxygen and nitrogen species.

a reduction in TAPSE and RVEF compared with the PBS group. Furthermore, RV systolic blood pressure (RVSP) and RV/(LV+S) were significantly higher in the Cig+Ova group. However, miR-135a/b-5p effectively counteracted cigarette and ovalbumin-induced right ventricular hypertrophy, as indicated in Table 1.

## Discussion

The central role of Ca<sup>2+</sup> signaling in agonist-elicited intrinsic contraction force generation in airway smooth

muscle has been established (Wylam et al., 2012). Furthermore, it is a well-known pathway in mediating airway SM cell proliferation. However, the precise signaling and transduction events that link the regulation of [Ca<sup>2+</sup>]<sub>i</sub> and cigarette-induced airway response are not fully established. Therefore, identifying the molecular mechanisms for nicotine-induced alterations in bronchial smooth muscle cells could offer insights into COPD pathogenesis and treatment. We found an ~two-fold increase in TRPC6 protein expression in COPD samples compared with healthy samples (Fig. 7A). IHC results further confirm the high

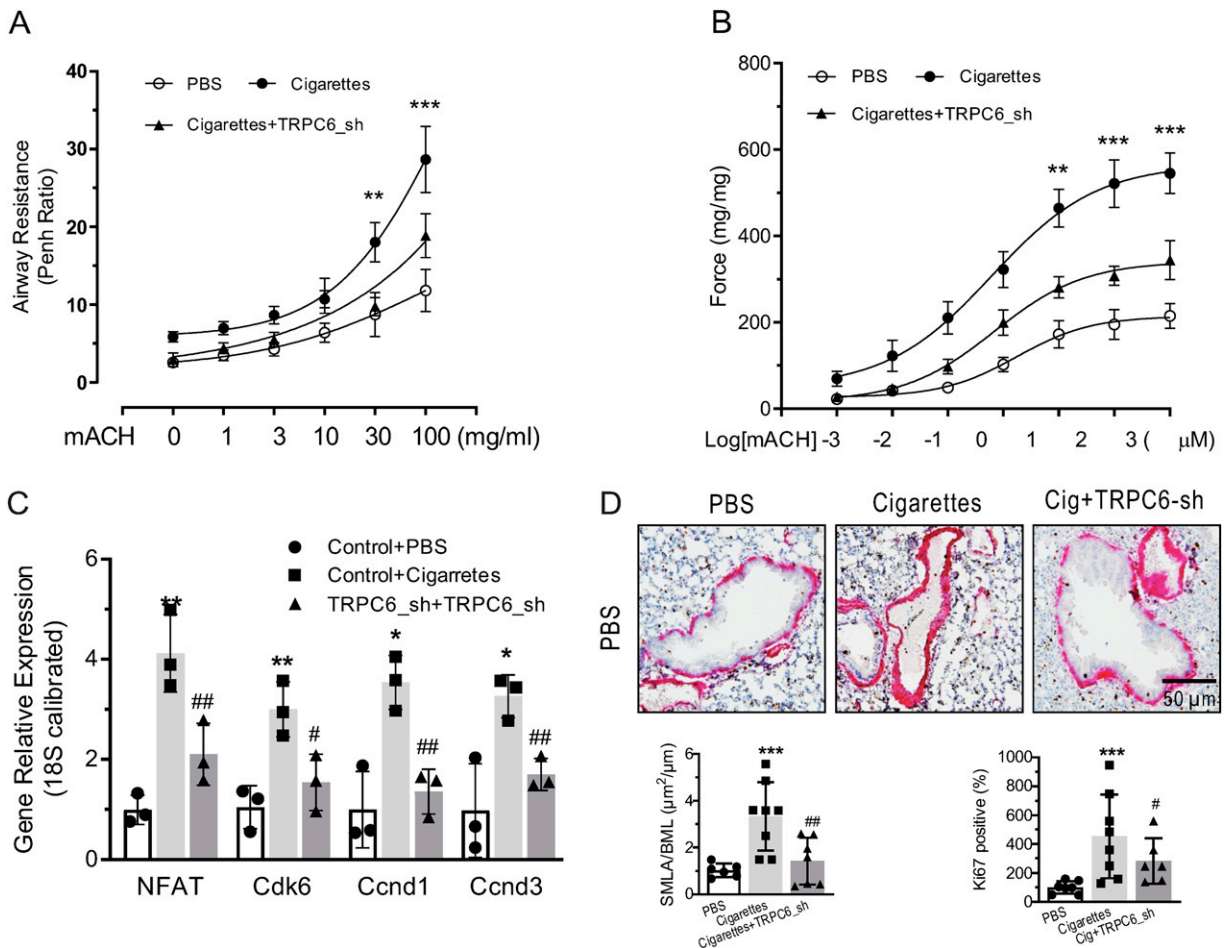


**FIG. 5. TRPC6 knockdown alleviates cigarette smoke-induced ASM hyperresponsiveness and remodeling in mice.** (A) inhalation of cigarette smoke exacerbated the methacholine-induced increase in airway hyperresponsiveness as measured by Penh using a noninvasive unrestricted whole-body plethysmography system. Mice exposed to cigarette smoke showed a significant increase in Penh. Knockdown of TRPC6 ameliorates cigarette smoke, causing a significant increase in Penh in mice. (B) Inhalation of cigarette smoke also intensified the methacholine-induced increase in airway contraction, as determined by *in vitro* airway muscle contractile responses to mACh in isolated tracheal rings. Mice exposed to cigarette smoke showed a significant increase in contraction compared with mice administered with PBS. Knockdown of TRPC6 in mice exposed to cigarette smoke resulted in a significant decrease in contraction. (C) Cigarette smoke exposure and TRPC6 influenced the expression of NFAT and its target genes in airway smooth muscle. mRNA levels of NFAT and its target genes were measured using real-time qPCR in airway smooth muscle collected from the mice mentioned above. (D) Immunohistochemistry co-staining of  $\alpha$ -smooth muscle actin (pink) and Ki67 (brown) were conducted in airways from the mice model mentioned above. The arrows indicate the co-localization of  $\alpha$ -smooth muscle actin and Ki67. The lower panel normalizes the smooth muscle layer area to the basement membrane length (SMLA/BML) and Ki67 positive cells to total cells from the upper panel. \* $p < 0.05$ , \*\* $p < 0.01$ , \*\*\* $p < 0.001$ , compared with the PBS group; # $p < 0.05$ , ## $p < 0.01$  compared with the cigarettes group. NFAT, nuclear factor of activated T-cells.

expression of TRPC6 in COPD samples (Fig. 7B). Our study is the first to demonstrate that miR-135a/b-5p expression is downregulated in a panel of bronchial smooth muscle tissue from patients with COPD compared with normal donors. Although several targets of miR-135a/b-5p have been biologically verified, none have been proven in HASMCs (Goto et al., 2014; Qin et al., 2010). Despite inter-individual variation in miR-135a/b-5p and TRPC6 expression across our sample set, a significant inverse correlation was observed between normal and COPD bronchial smooth muscle tissue, suggesting that TRPC6 channel expression was downregulated by miR-135a/b-5p *in vivo* as well. However, the effect of miR-135a/b-5p on TRPC6 alone is not sufficient to fully

explain the observed phenotypic effects. It is important to note that miR-135a/b-5p will undoubtedly have an impact on several other targets that control the cell growth. The precise balance of the interactions discussed here will determine the overall functionality of miR-135a/b-5p in the cell and explain its apparent ability to act in contrasting fashions in different diseases.

The extract of cigarette smoking contains complex components. Numerous studies have already confirmed that long-term exposure to cigarette extract can cause oxidative damage to lung epithelial cells (Cipollina et al., 2022). However, one of the main components of cigarette extract is nicotine. Our focus is on how low-dose, long-term nicotine



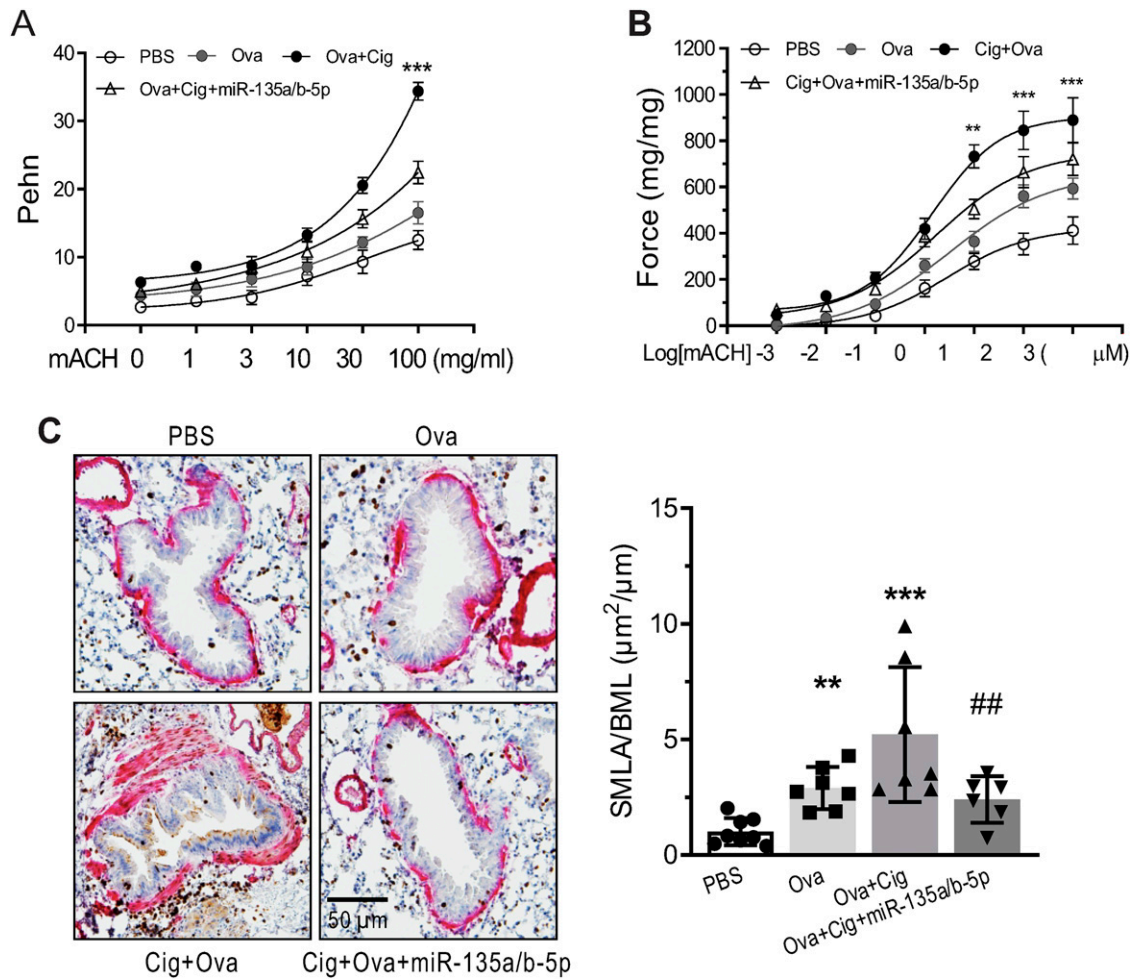


**FIG. 6. The impact of miR-135a/b-5p in a murine model of asthma-COPD overlap syndrome.** (A) Treatment with ovalbumin and inhalation of cigarette smoke resulted in increased methacholine-induced airway resistance. Mice that received a tail-vein injection of lentivirus particles containing miR-135a/b-5p exhibited significantly reduced ovalbumin, and cigarette smoke caused airway resistance. (B) *In vitro* airway muscle contractile responses to mACh were greatly reduced in the isolated airway (tracheal) rings from mice injected with miR-135a/b-5p lentivirus particles. (C) Immunohistochemistry co-stains of  $\alpha$ -smooth muscle actin (pink) and Ki67 (brown) in the airways. The right panel normalizes the smooth muscle layer area to the basement membrane length (SMLA/BML) from the left panel. The results suggest that miR-135a/b-5p treatment significantly decreased airway smooth muscle proliferation.  $**p < 0.01$ ,  $***p < 0.001$ , compared with the PBS group;  $##p < 0.01$  compared with the Ova + Cig group.

exposure affects airway smooth muscle and exploring the underlying molecular mechanisms. Our results show that low-dose, long-term treatment can induce a phenotypic transformation of airway smooth muscle cells from a contractile/quiescent to a synthetic/proliferative type by increasing general ROS levels. In addition, the *Tpc6* level in mice heart samples was significantly lower than lung samples in pulmonary vascular remodeling models (Supplementary Fig. S5A). Moreover, the Gene Expression Database, collecting and integrating the gene expression information in Mouse Genome Informatics built by The Jackson Laboratory, has shown that endogenous *Tpc6* expression in the heart ventricle was absent, whereas it was present in lung and respiratory tract during mouse development (Supplementary Fig. S5B). We believe that the low expression of TRPC6 in the ventricles results in it being poorly regulated by miR-135a/b-5p in cardiac muscle cells. We conclude that miR-135a/b-5p effectively counteracted cigarette and ovalbumin-induced

right ventricular hypertrophy by improving pulmonary vascular remodeling. Taken together, our results describe a novel pathway in which HASMCs exposed to nicotine promote proliferation through nicotine  $\rightarrow \alpha 7$  nAChR  $\rightarrow$  RONS  $\rightarrow$  NF- $\kappa$ B  $\rightarrow$  TRPC6  $\rightarrow$  NFAT signaling, which has not been reported previously (Fig. 7C). We propose a model in which nicotine, via NF- $\kappa$ B and miR-135a/b-5p, enhances TRPC6 expression and activation in ASM, leading to a phenotype switch from a contractile/quiescent to a synthetic/proliferative type.

## Materials and Methods

### Cell culture and transient transfection

HASMCs obtained from normal participants and patients with COPD were cultured in SmBM medium (Lonza, cat#: CC-3181) and SmGM-2 Bullet Kit (Lonza, cat#: CC-3182), respectively. The cells were maintained at 37°C in a humidified atmosphere containing 5% CO<sub>2</sub>. HEK-293T cells

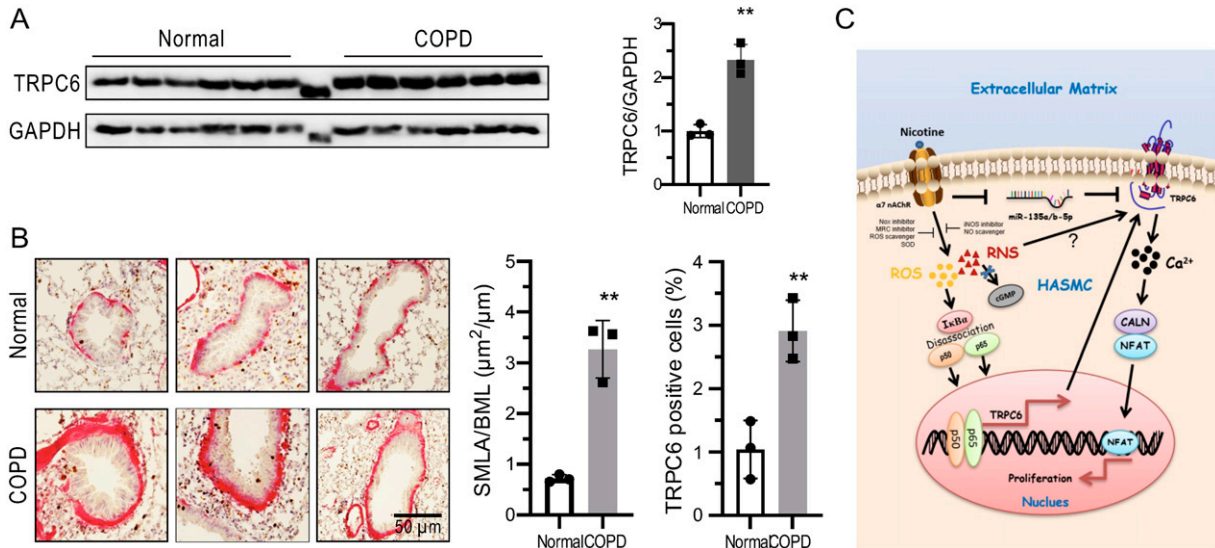


**FIG. 7. TRPC6 channel protein expression in human samples.** (A) Western blot analysis revealed a significant increase in TRPC6 protein expression in bronchial tissue isolated from patients with COPD compared with normal donors. The densitometric analysis confirmed a statistically significant difference (right panel). (B) Immunohistochemistry co-stains of  $\alpha$ -smooth muscle actin and TRPC6 in bronchial tissue isolated from normal donors and patients with COPD illustrated colocalization of TRPC6 with  $\alpha$ -smooth muscle actin. The right panels normalize the smooth muscle layer area to the basement membrane length (SMLA/BML) and TRPC6-positive cells to total cells from the left panels. \*\* $p < 0.01$ , \*\*\* $p < 0.005$ . (C) A schematic model depicted the critical role of miR-135a/b-5p- and NF- $\kappa$ B-dependent TRPC6 channels in COPD. In HASMCs, nicotine triggered the indicated signaling cascades, leading to the translocation of p65 and p50 through the  $\alpha 7$  nAChR ROS-dependent pathway. This led to the sustained activation of transcriptional signaling, increasing TRPC6 expression, and a decrease in miR-135a/b-5p. The direct influx of  $\text{Ca}^{2+}$  was activated, followed by the induction of downstream gene activation of NFAT signaling, leading to HASMCs proliferation and migration. CALN, calcineurin; MRC, mitochondrial respiratory chain; Nox, NADPH oxidase; NO, nitric oxide; NOS, nitric oxide synthase; RNS, reactive nitrogen species; SOD, superoxide dismutase.

obtained from the American Type Culture Collection were grown in DMEM (Life Technologies, cat#: 10-013-cv) supplemented with 10% fetal bovine serum (Hyclone, cat#: SH30071.03) and 10  $\mu\text{g}/\text{mL}$  penicillin and streptomycin. Transfection of 293T cells was performed using Lipofectamine 2000 (Invitrogen, cat#: 11668-027). Transient transfections of HASMCs were performed by electroporation using the Nucleofector Primary Smooth Muscle Cells Kits

and Instrument (Lonza, amaxa). Specifically,  $1 \times 10^6$  HASMCs were mixed with 100  $\mu\text{L}$  of the nucleofector solution containing 1–10  $\mu\text{g}$  DNA and transferred to a cuvette. Program U-25 was applied, and after treatment, the cells were immediately plated out in pre-warmed medium into six-well plates and the medium was changed 24 h later.

#### Production of lentivirus

The following lentiviral products were utilized: GIPZ Lentiviral Human TRPC6 shRNAs (V2LHS\_171560) from Dharmacon, Human TRPC6 lentiviral overexpression plasmid (VB151104-10021) from Vectorbuilder, smooth muscle cell-specific mouse TRPC6 shRNA from Biosettia, mouse miR-135a/b-5p lentiviral overexpression plasmid (mm10720) from Applied Biological Materials, and GIPZ Lentiviral Human p65/50 shRNA (V2LHS\_98065/V2LHS\_201509) targeting human NF- $\kappa$ B from Dharmacon. Lentivirus packaging was performed using the standard procedure, with oligonucleotide sequences for shRNA provided in Supplementary Table S2. Briefly, 293FT cells were cultured in DMEM and incubated with the recombinant lentiviral plasmid, pCMV-dR8.2 dvpr, and pCMV-VSV-G in  $\text{CaCl}_2$  and HEPES-buffered medium. The medium was collected and replenished at 48 and 72 h after transfection, and the lentivirus was concentrated using an Amicon Ultra centrifugal filter (Millipore, cat#: UFC903024) before being stored at  $-80^\circ\text{C}$ . Lentivirus titration was  $10^8$  transforming units/mL.

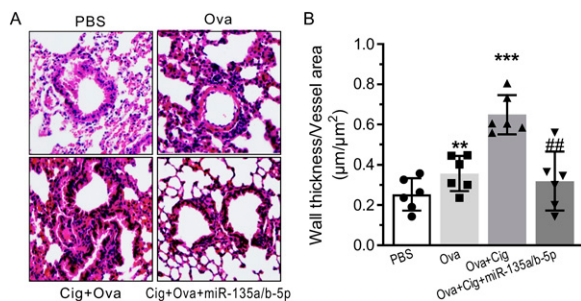


**FIG. 8. miR-135a/b-5p attenuates cigarette and ovalbumin-induced pulmonary vascular remodeling in mice.** (A) Hematoxylin and eosin staining of pulmonary arterioles of mice illustrated the effect of miR-135a/b-5p on pulmonary vessel wall thickness. (B) miR-135a/b-5p significantly reduced pulmonary vessel wall thickness in mice exposed to cigarette smoke and ovalbumin by normalizing the wall thickness to the vessel area. Data are presented as mean  $\pm$  SD, \*\* $p < 0.01$  compared with the PBS group, ### $p < 0.01$  compared with the Cig + Ova group.

TABLE 1. CARDIAC HEMODYNAMICS, ECHOCARDIOGRAPHY, AND RIGHT VENTRICULAR HYPERTROPHY INDEX OF MICE IN EACH GROUP

Group	PBS	Ova	Cig + Ova	Cig + Ova + miR-135a/b-5p
RVEDD (mm)	2.39 ± 0.891	3.27 ± 1.025	5.67 ± 1.63 <sup>***</sup>	3.83 ± 0.031 <sup>##</sup>
TAPSE (mm)	0.265 ± 0.052	0.275 ± 0.015	0.131 ± 0.073 <sup>**</sup>	0.182 ± 0.026 <sup>#</sup>
RVEF (%)	44.51 ± 3.73	46.724 ± 3.72	36.27 ± 1.251 <sup>**</sup>	44.73 ± 3.73 <sup>##</sup>
RVSP (mmHg)	16.47 ± 1.62	16.906 ± 2.542	35.524 ± 3.56 <sup>***</sup>	24.733 ± 2.547 <sup>###</sup>
RV/(LV+S)	0.142 ± 0.167	0.154 ± 0.054	0.306 ± 0.014 <sup>***</sup>	0.265 ± 0.692 <sup>#</sup>

\* $p < 0.05$ , \*\* $p < 0.01$ , \*\*\* $p < 0.001$ , compared with the PBS group.

<sup>#</sup> $p < 0.05$ , <sup>##</sup> $p < 0.01$ , <sup>###</sup> $p < 0.001$ , compared with the Cig + Ova group.

#### Label-free image-based 2D cell proliferation assay

Normal or COPD HASMCs were seeded into 96-well plates and cultured for indicated days. The 96-well plate was placed in the BIOSPA |8 automated incubator, previously set to 37°C and 5% CO<sub>2</sub>. Time-lapse imaging of the cell areas was performed every 24 h over 8 days using phase contrast and a 4× objective. The CYTATION |1 imaging reader, Gen5™ 3.0 Microplate Reader and Imager Software were used for the automated image capturing and analysis system. Image acquisition is completely automated from sample translation, focusing, and exposure control. The included cell analysis tool calculates precise values in variable parameters, *e.g.*, object area and size, as well as the object intensity. The customized transformation tool can convert the calculated values into the preferred presentation method. Six independent experiments were conducted.

#### Migration assays

Briefly, HASMCs were seeded on an 8 μm pore size transwell filter insert (FALCON, REF 353182) coated with 40 μg/mL collagen type 1 (CORNING, REF 354236). After incubating the cells for 3–4 h at 37°C, those adhering to the upper surface of the filter were removed using a cotton applicator. Subsequently, the cells were fixed with 3.7% formaldehyde, and stained with crystal violet, and the number of cells on the bottom was counted. The data presented herein are collected from at least three experiments conducted in triplicate.

#### Immunoprecipitation and Western blot

HASMCs were collected and lysed using immunoprecipitation (IP) lysis buffer, which included 20 mM HEPES, pH 8.0, 0.2 mM EDTA, 5% glycerol, 150 mM NaCl, and 1% NP40. After clarification, 0.5 mg of lysate was subjected to IP with 2 μg of anti-IκBα antibody (Santa Cruz, cat#: sc-371) at 4°C overnight, with a control group using 20 μl of rabbit or mouse IgG. Protein A or G magnetic beads were added to capture the immune complex for 3 h at 4°C. The immune complexes were washed three times with IP lysis buffer, subjected to 10% SDS-PAGE, and then transferred onto a PVDF membrane (GE Healthcare). Subsequently, Western blotting was conducted using various primary antibodies, including rabbit anti-TRPC6 (1:1000 dilution; Alomone Laboratories, #ACC-016), anti-p65 (1:1000 dilution, Santa Cruz, cat#: sc-372), anti-p50 (1:1000 dilution, Santa Cruz, cat#: sc-7178), anti-lamin A (1:1000 dilution; Abcam), anti-GAPDH (1:1000 dilution; Santa Cruz), and GAPDH

(1:1000 dilution; Santa Cruz Biotechnology). The secondary antibody used was horseradish peroxidase (HRP)-conjugated goat-anti-rabbit IgG antibody or goat-anti-mouse IgG antibody (NA934V, GE Healthcare), followed by the visualization of protein bands using an enhanced chemiluminescence reagent (Santa Cruz, cat#: sc-2048) and the LAS-3000 image system (Fujifilm, Tokyo, Japan).

#### EMSA

Unlabeled single-stranded wild-type NF-κB probe (NF-κB-WT) and mutant NF-κB probe (NF-κB-MT) were procured from IDT (refer to Supplementary Table S3). Biotinylation was performed on the 3' terminus of the probe using the Biotin 3' End DNA Labeling kit (Thermo Scientific, No.89818). For probe mobility shift assays, 8 μg of nuclear extract protein was incubated with 1 μg of poly(dI•dC) and 2 nM of biotin-labeled NF-κB-WT probe in the binding buffer at room temperature for 20 min. For antibody supershift assays, 8 μg of nuclear protein was initially mixed with 2 nM biotin-labeled NF-κB WT probe for 20 min, followed by incubation with 2 μg of either anti-p65 antibody or normal rabbit IgG (Santa Cruz, CA, USA) at room temperature for 1 h. To assess probe competition, a 200-fold excess of unlabeled competitor probes was added and allowed to incubate with 8 μg of nuclear proteins for 20 min. Subsequently, 2 nM of biotin-labeled NF-κB-WT probe was added and incubated for an additional 20 min at room temperature. To demonstrate the inability of specific nuclear protein binding by NF-κB-MT probe, 8 μg of nuclear protein was incubated with 2 nM biotin-labeled NF-κB-MT probe for 20 min, followed by the addition of 2 nM biotin-labeled NF-κB probe and incubated for an additional 20 min at room temperature. The reactions were electrophoresed on a 6% non-denaturing polyacrylamide gel at 100 V for 1 h and transferred to a nylon membrane (Thermo Scientific, cat#: 77016). Detection of the biotin-labeled DNA was performed using the Light-Shift chemiluminescent electrophoretic mobility shift assay kit (Thermo Scientific, cat#: 20148) and chemiluminescent nucleic acid detection module (Thermo Scientific, cat#: 89880).

#### Luciferase reporter gene assays

Hek-293T cells were transfected with a luciferase construct driven by either NF-κB or TRPC6 promoter and a control renilla luciferase construct at a ratio of 20:1. The luciferase activity was measured using the Dual-Luciferase System (Promega, E1910) according to the manufacturer's instructions. To create TRPC6-3'-UTR luciferase reporters,



TRPC6-3'-UTR FL and truncated TRPC6-3'-UTR were amplified from TRPC6 overexpression plasmid (3'-UTR included) using PCR amplification with the Phusion DNA Polymerase (Thermo Scientific, F530S) and appropriate primers (see list of primers used for the construction of luciferase reporters). The resultant PCR fragments were subcloned into the pmiR-target vector, generating TRPC6-3'-UTR-FL-luc, TRPC6-3'-UTR-1-576-luc, and TRPC6-3'-UTR-1-598-luc.

#### *Measurement of intercellular ROS*

Intracellular ROS was measured using a specific cell-permeable red fluorescence dye (Abcam#: ab186027) and green fluorescent dye chloromethyl dihydrochlorofluorescein diacetate (CM-H2DCF-DA) (Molecular Probes™, cat#: C6827). Briefly, freshly isolated cells were loaded with cell-permeable red fluorescence dye or CM-H2DCF-DA (5  $\mu$ M) at 37°C for 30 min according to the manufacturer's procedure. Subsequently, the cells were rinsed with a prewarmed, dye-free bath solution for 15 min, allowing the conversion of intracellular dye into its nonester form while washing out the extracellular dye. The assays were performed by microplate fluorometry (Ex/Em = 520/605 nm for red fluorescence and Ex/Em = 488/510 nm for green fluorescence), and fluorescence intensity was reported in arbitrary units (a.u.).

#### *Nitrite level determination by colorimetric assays*

NO is a gaseous free radical with a short life, and no available methods to measure NO levels directly exist. Therefore, the levels of more stable NO metabolites (nitrite, NO<sub>2</sub><sup>-</sup>) were measured in cell culture supernatants using the NO colorimetric assay (R&D Systems, Catalog #: KGE001). In brief, NO production was determined by estimating the concentration of nitrite (NO<sub>2</sub><sup>-</sup>) in the cell media using Griess reagent (R&D Systems Inc.). The supernatant was stored in an incubator for 15 min at room temperature. The activities were assessed on a spectrometer ( $\lambda$  = 540 nm). All evaluation was conducted with three trials.

#### *Intracellular calcium ([Ca<sup>2+</sup>]<sub>i</sub>) detection*

According to the manufacturer's protocol, intracellular calcium was measured using Calcium Quantification Kit-Red Fluorescence (Abcam, cat#: ab112115). Briefly, prepare a calcium standard by diluting the appropriate amount of the 300 mM calcium standard into H<sub>2</sub>O to produce a calcium concentration ranging from 0 to 3 mM (12 mg/dL). Add 50  $\mu$ L of serially diluted calcium standard into each well. Add 50  $\mu$ L of the assay reaction mixture to each well of calcium standard, blank control, and test samples to make the total calcium assay volume of 100  $\mu$ L/well. Incubate the reaction for 5–30 min at room temperature, protected from light. Monitor the fluorescence intensity with a fluorescence plate reader at Ex/Em = 540/590 nm.

#### *Preparation of the mouse model for cigarette smoke challenge and ovalbumin sensitization*

The study involving animals was reviewed and approved by the Committee of Care and Use of Animals of the First People's Hospital of Lianyungang. To prepare the mouse

model, conscious C57BL/6 mice were exposed to cigarette smoke through inhalation for 60 consecutive days, where they were placed in an exposure chamber for 1 h per day. In addition, mice aged 6–7 weeks were sensitized by intraperitoneal injection of a mixture of aluminum hydroxide, 0.6 mg of ovalbumin, and 0.9% saline solution. From days 15 to 19, the mice were challenged with intranasal instillation of ovalbumin (0.3 mg/mL, 50  $\mu$ L). Control mice were treated with 0.9% saline solution only. After the final intranasal exposure to ovalbumin or saline, airway muscle contractile responses to the muscarinic agonist methacholine were determined by measuring enhanced pause (Penh) using an unrestricted whole-body plethysmograph system.

#### *Measurement of muscle contraction*

To examine airway muscle contractile responses to methacholine, isolated tracheal rings were prepared using the tissue bath technique. The trachea was removed from the connective and epithelial tissue, and four cartilage tracheal rings were obtained from the distal tracheae. The tracheal rings were then placed in 2-ml tissue bath chambers, held in aerated PSS containing 21% O<sub>2</sub>, 5% CO<sub>2</sub>, and 74% N<sub>2</sub>, and warmed to 37°C. The resting tone was set at 250 mg, and the contractile force was recorded using a PowerLab/4SP recording system with a highly sensitive force transducer.

#### *Immunohistochemistry*

For the examination of isolated mouse lung lobes, antigen-antibody complexes were labeled using an avidin-biotinylated enzyme complex (VECTASTAIN® ABC AP Kits, cat#: AK-5200) and 3,3-diaminobenzidine substrate kit (VECTASTAIN® Original ABC-HRP Kits, cat#: SK-4001). Sections of 4 mm thickness were sliced and immunostained with an anti- $\alpha$ -SM actin antibody (Abcam, cat#: ab5694) combined with anti-Ki67 (Abcam, cat#: ab833) or TRPC6 antibody (Abcam, cat#: ab62461) at concentrations of either 1:400 or 1:600. The sections were visualized using an Olympus microscope, and the area of the smooth muscle layer was calculated using ImageJ software and expressed as the area (in pink) per square millimeter of bronchiole ring. A percentage of Ki67 or TRPC6-positive cells was calculated by dividing the number of cells with Ki67 or TRPC6-positive nuclei by the total number of cells with a hematoxylin-positive nucleus.

#### *Hemodynamics and ventricular weight measurements*

After echocardiography, a transthoracic RV puncture was conducted to measure RVSP. This was done by inserting a needle through the intercostal space of the chest wall and connecting it to a micro pressure sensor (ALCB10 cardiac function analysis system, Shanghai Alcott Biotechnology Co. Ltd.). The pressure in the right ventricle was recorded for 10 consecutive beats to estimate pulmonary artery pressure. The heart was then rapidly dissected, and the LV wall, interventricular septum (S), and RV wall were weighed separately. The right ventricular hypertrophy index (RVHI), *i.e.*, the RV to (LV+S) wet weight ratio, was utilized to assess right ventricular hypertrophy.

### Ethics statement

The research on human tissue samples was conducted with the consent of the participants and approved by a Research Ethics Committee (REC) of the First People's Hospital of Lianyungang.

### Specification of electronic laboratory notebook

Electronic laboratory notebook was not used in this study.

### Statistical analysis

All data are expressed as mean  $\pm$  SEM. Statistical analysis was conducted using GraphPad Prism software. Paired Student's *t*-test was used to compare data before and after treatment in the same sample, unpaired (independent) Student's *t*-test for two-sample comparisons, one-way ANOVA with an appropriate *post hoc* test for multiple-sample comparisons, and two-way ANOVA for comparisons of the means of populations classified in two different ways or the mean responses in an experiment with two factors. Results with a *p* value of  $< 0.05$  were considered statistically significant.

### Authors' Contribution

Conception and design: K.L. and Y.F.Z. Experiments carried out: K.L., Q.M.T., and J.Z. K.L. and Q.M.T. performed studies on molecular mechanisms and function. J.Z. performed the experiments on the smoking mouse model. Analysis of the human sample: G.H.L. Data interpretation and discussion: K.L. and Y.F.Z.

### Data Availability Statement

All data supporting the findings of this study are available in the article and its Supplementary Information section.

### Patient Consent for Publication

All clinical specimens were obtained from surgically resected tissues of patients between 2018 and 2023 at the First People's Hospital of Lianyungang (Lianyungang, China), and all patients provided signed informed consent. The clinical subject study was approved by The Research Ethics Committee of the First People's Hospital of Lianyungang.

### Ethics Statement

This study was approved by the ethical review board of the First People's Hospital of Lianyungang. All patients were given and accepted an informed consent form before their enrollment.

### Author Disclosure Statement

The authors declare that they have no competing interests.

### Funding Information

This work was supported by Lianyungang Municipal Health Commission (No. 202009).

### Supplementary Material

Supplementary Figure S1

Supplementary Figure S2  
Supplementary Figure S3  
Supplementary Figure S4  
Supplementary Figure S5  
Supplementary Table S1  
Supplementary Table S2  
Supplementary Table S3  
Supplementary Table S4

### References

- Benza RL, Grünig E, Sandner P, et al. The nitric oxide-soluble guanylate cyclase-cGMP pathway in pulmonary hypertension: From PDE5 to soluble guanylate cyclase. *Eur Respir Rev* 2024;33(171):230183; doi: 10.1183/16000617.0183-2023
- Boulay G, Zhu X, Peyton M, et al. Cloning and expression of a novel mammalian homolog of *Drosophila* Transient Receptor Potential (Trp) involved in calcium entry secondary to activation of receptors coupled by the Gq class of G protein. *J Biol Chem* 1997;272(47):29672–29680; doi: 10.1074/jbc.272.47.29672
- Christenson SA, Steiling K, van den Berge M, et al. Asthma-COPD overlap. Clinical relevance of genomic signatures of type 2 inflammation in chronic obstructive pulmonary disease. *Am J Respir Crit Care Med* 2015;191(7):758–766; doi: 10.1164/rccm.201408-1458OC
- Cipollina C, Bruno A, Fasola S, et al. Cellular and molecular signatures of oxidative stress in bronchial epithelial cell models injured by cigarette smoke extract. *Int J Mol Sci* 2022; 23(3):1770; doi: 10.3390/ijms23031770
- Ezzie ME, Crawford M, Cho JH, et al. Gene expression networks in COPD: MicroRNA and mRNA regulation. *Thorax* 2012;67(2):122–131; doi: 10.1136/thoraxjnl-2011-200089
- Garcia RL, Schilling WP. Differential expression of mammalian TRP homologues across tissues and cell lines. *Biochem Biophys Res Commun* 1997;239(1):279–283; doi: 10.1006/bbrc.1997.7458
- Goto Y, Kojima S, Nishikawa R, et al. The microRNA-23b/27b/24-1 cluster is a disease progression marker and tumor suppressor in prostate cancer. *Oncotarget* 2014;5(17): 7748–7759; doi: 10.18632/oncotarget.2294
- Gudermann T, Mederos y Schnitzler M, Dietrich A. Receptor-operated cation entry—more than esoteric terminology? *Sci STKE* 2004;2004(243):pe35; doi: 10.1126/stke.2432004pe35
- He F, Peng F, Xia X, et al. MiR-135a promotes renal fibrosis in diabetic nephropathy by regulating TRPC1. *Diabetologia* 2014;57(8):1726–1736; doi: 10.1007/s00125-014-3282-0
- Kano Y, Tanabe T, Nagasawa J, et al. Effect of age on rat aortic responses to acetylcholine and Nitric Oxide Donor (NOC-18). *Res Commun Mol Pathol Pharmacol* 2000;107(3–4):331–334.
- Liao Y, Plummer NW, George MD, et al. A role for Orai in TRPC-mediated Ca<sup>2+</sup> entry suggests that a TRPC:Orai complex may mediate store and receptor operated Ca<sup>2+</sup> entry. *Proc Natl Acad Sci U S A* 2009;106(9):3202–3206; doi: 10.1073/pnas.0813346106
- Mannino DM, Buist AS. Global burden of COPD: Risk factors, prevalence, and future trends. *Lancet* 2007;370(9589): 765–773; doi: 10.1016/S0140-6736(07)61380-4
- Müller M, Essin K, Hill K, et al. Specific TRPC6 channel activation, a novel approach to stimulate keratinocyte differentiation. *J Biol Chem* 2008;283(49):33942–33954; doi: 10.1074/jbc.M801844200

- Qin W, Shi Y, Zhao B, et al. miR-24 regulates apoptosis by targeting the open reading frame (ORF) region of FAF1 in cancer cells. *PLoS One* 2010;5(2):e9429; doi: 10.1371/journal.pone.0009429
- Riccio A, Medhurst AD, Mattei C, et al. mRNA distribution analysis of human TRPC family in CNS and peripheral tissues. *Brain Res Mol Brain Res* 2002;109(1–2):95–104; doi: 10.1016/s0169-328x(02)00527-2
- Stolk J, Hiltermann TJ, Dijkman JH, et al. Characteristics of the inhibition of NADPH oxidase activation in neutrophils by apocynin, a methoxy-substituted catechol. *Am J Respir Cell Mol Biol* 1994;11(1):95–102; doi: 10.1165/ajrcmb.11.1.8018341
- Svobodova B, Groschner K. Reprint of “Mechanisms of lipid regulation and lipid gating in TRPC channels. *Cell Calcium* 2016;60(2):133–141; doi: 10.1016/j.ceca.2016.06.010
- Tang W, Jiang Y, Mu X, et al. MiR-135a functions as a tumor suppressor in epithelial ovarian cancer and regulates HOXA10 expression. *Cell Signal* 2014;26(7):1420–1426; doi: 10.1016/j.cellsig.2014.03.002
- Tannus-Silva DG, Rabahi MF. State of the art review of the right ventricle in COPD Patients: It is time to look closer. *Lung* 2017;195(1):9–17; doi: 10.1007/s00408-016-9961-5
- Ten Broeke R, Blalock JE, Nijkamp FP, et al. Calcium sensors as new therapeutic targets for asthma and chronic obstructive pulmonary disease. *Clin Exp Allergy* 2004;34(2):170–176; doi: 10.1111/j.1365-2222.2004.01908.x
- Weissmann N, Dietrich A, Fuchs B, et al. Classical Transient Receptor Potential Channel 6 (TRPC6) is essential for hypoxic pulmonary vasoconstriction and alveolar gas exchange. *Proc Natl Acad Sci U S A* 2006;103(50):19093–19098; doi: 10.1073/pnas.0606728103
- Wu X, Tang X, Xian M, et al. Synthesis and cytotoxicities of mannose conjugated S-nitroso-N-acetylpenicillamine (SNAP). *Bioorg Med Chem* 2002;10(7):2303–2307; doi: 10.1016/s0968-0896(02)00064-0
- Wylam ME, Xue A, Sieck GC. Mechanisms of intrinsic force in small human airways. *Respir Physiol Neurobiol* 2012;181(1):99–108; doi: 10.1016/j.resp.2012.01.011
- Xu SZ, Sukumar P, Zeng F, et al. TRPC channel activation by extracellular thioredoxin. *Nature* 2008;451(7174):69–72; doi: 10.1038/nature06414
- Yamada Y, Hidaka H, Seki N, et al. Tumor-suppressive microRNA-135a inhibits cancer cell proliferation by targeting the c-MYC oncogene in renal cell carcinoma. *Cancer Sci* 2013;104(3):304–312; doi: 10.1111/cas.12072
- Yoshida T, Inoue R, Morii T, et al. Nitric oxide activates TRP channels by cysteine S-nitrosylation. *Nat Chem Biol* 2006;2(11):596–607; doi: 10.1038/nchembio821

Address correspondence to:

Dr. Yun-Feng Zhao

Department of Cardiology

The First People's Hospital of Lianyungang

The Affiliated Lianyungang Hospital of

Xuzhou Medical University

182 Tongguan North Road

Lianyungang

Jiangsu Province 222000

China

E-mail: liukun2023@stu.njmu.edu.cn

Date of first submission to ARS Central, February 2, 2024; date of final revised submission, September 27, 2024; date of acceptance, October 5, 2024.

### Abbreviations Used

ASMCs	= airway smooth muscle cells
ASM	= Airway smooth muscle
cGMP	= Cyclic guanosine monophosphate
COPD	= chronic obstructive pulmonary disease
DMEM	= Dulbecco's Modified Eagle Medium
EDTA	= Ethylenediaminetetraacetic acid
EMSA	= electrophoretic mobility shift assays
GSEA	= Gene Set Enrichment Analysis
HEPES	= 2-[4-(2-hydroxyethyl)piperazin-1-yl]ethanesulfonic acid
IDT	= Integrated DNA Technologies
IHC	= Immunohistochemistry
MASMCs	= mouse airway smooth muscle cells
miR-135a/b-5p	= microRNA-135a/b-5p
MTS	= [3-(4,5-dimethylthiazol-2-yl)-5-(3-carboxymethoxyphenyl)-2-(4-sulfophenyl)-2H-tetrazolium, inner salt]
NFAT	= nuclear factor of activated T-cells
NP40	= nonyl phenoxypolyethoxyethanol 40
NRE	= NF- $\kappa$ B response element
PASMCs	= pulmonary artery smooth muscle cells
PBS	= Phosphate-buffered saline
PVDF	= Polyvinylidene fluoride
ROS	= reactive oxygen species
RT-qPCR	= reverse transcription quantitative polymerase chain reaction
SDS-PAGE	= Sodium dodecyl sulfate-polyacrylamide gel electrophoresis
TRPC6	= transient receptor potential channel 6